PAMM · Proc. Appl. Math. Mech. **17**, 383 – 384 (2017) / **DOI** 10.1002/pamm.201710161

Phase Field Modeling of Ductile Fracture in Soil Mechanics

Fadi Aldakheel[1,*], **Daniel Kienle**[1], **Marc-André Keip**[1], and **Christian Miehe**[1]

[1] Institute of Applied Mechanics (CE), Chair I, University of Stuttgart, Pfaffenwaldring 7, 70569 Stuttgart, Germany

This work outlines a rigorous framework for the ductile failure of frictional materials in elastic-plastic soil mechanics undergoing large strains. Describing soil crack formation can be achieved in a convenient way by recently developed continuum phase field approaches to fracture, which are based on the regularization of sharp crack discontinuities [1]. This avoids the use of complex discretization methods for crack discontinuities, and can account for complex crack patterns. For frictional materials, a *non–associative* Drucker–Prager-type elastic-plastic constitutive model suitable for a wide range of applications in soil mechanics is developed. It is linked to a failure criterion in terms of the elastic-plastic work density that drives the fracture phase field. We demonstrate the modeling capabilities and algorithmic performance of the proposed formulation by a representative numerical example that describes soil crack formation using elastic-plastic fracture mechanics.

1 Constitutive formulation of the multi-field problem

The ductile failure response of frictional materials is described by the deformation map $\boldsymbol{\varphi}$ and the crack phase field d as global primary fields. The plastic strain $\boldsymbol{\varepsilon}^p$ and the equivalent plastic strain α are the local internal variables. The free energy density function of the coupled problem reads

$$\widehat{\Psi}(\boldsymbol{\varepsilon}^e, \alpha; d) = \widehat{\Psi}_e(\boldsymbol{\varepsilon}^e; d) + \widehat{\Psi}_p(\alpha; d) \quad \text{with} \quad \boldsymbol{\varepsilon}^e := \boldsymbol{\varepsilon} - \boldsymbol{\varepsilon}^p \quad \text{and} \quad \boldsymbol{\varepsilon} := \frac{1}{2}\ln[(\nabla\boldsymbol{\varphi})^T(\nabla\boldsymbol{\varphi})] \,, \tag{1}$$

in terms of the logarithmic elastic strain measure $\boldsymbol{\varepsilon}^e$. The quadratic elastic part of the free energy function takes the form

$$\widehat{\Psi}_e(\boldsymbol{\varepsilon}^e; d) = (1-d)^2\psi_e^+(\boldsymbol{\varepsilon}^e) + \psi_e^-(\boldsymbol{\varepsilon}^e) \quad \text{with} \quad \psi_e^\pm(\boldsymbol{\varepsilon}^e) = \frac{\kappa}{2}\,\langle \mathrm{tr}[\boldsymbol{\varepsilon}^e]\rangle_\pm^2 + \mu\,\mathrm{tr}[\mathrm{dev}(\boldsymbol{\varepsilon}_\pm^e)^2] \tag{2}$$

with the bulk modulus $\kappa > 0$ and the shear modulus $\mu > 0$. The positive and negative elastic strain tensors are defined as $\boldsymbol{\varepsilon}_+^e := \sum_{a=1}^3 \langle \varepsilon_a^e\rangle_+ \, \boldsymbol{n}_a \otimes \boldsymbol{n}_a$ and $\boldsymbol{\varepsilon}_-^e := \boldsymbol{\varepsilon}^e - \boldsymbol{\varepsilon}_+^e$ with the ramp functions $\langle x\rangle_\pm := (x \pm |x|)/2$ of $\mathcal{R}_\pm$. The plastic contribution represents an isotropic hardening behavior and takes the form

$$\widehat{\Psi}_p = (1-d)^2\psi_p(\alpha) \quad \text{with} \quad \psi_p = \int_0^\alpha \widehat{y}(\widetilde{\alpha})\, d\widetilde{\alpha} \quad \text{and} \quad \widehat{y}(\alpha) = y_0 + h\alpha \tag{3}$$

in terms of the material parameters $y_0 > 0$ and $h \geq 0$, where the initial yield stress y_0 determines the threshold of the effective elastic response. Following Miehe et al. [2], the crack phase field $d \in [0,1]$ enters the energy function as a generalized internal variable. It governs the regularized crack surface functional Γ_l in terms of the crack surface density function γ_l

$$\frac{d}{dt}\Gamma_l(d) = \int_{\mathcal{B}} \delta_d\gamma_l(d,\nabla d)\,\dot{d}\; dV := \frac{1}{l_f}\int_{\mathcal{B}} [(1-d)\mathcal{H} - \eta\,\dot{d}]\cdot\dot{d}\, dV \geq 0 \quad \text{with} \quad \gamma_l(d,\nabla d) = \frac{1}{2l}d^2 + \frac{l}{2}||\nabla d||^2 \,. \tag{4}$$

Next, we define the non–associated Drucker–Prager-type yield criterion function for frictional materials in line with [3]

$$\widehat{\phi}(\boldsymbol{\sigma}, \beta_p) = \sqrt{\tfrac{3}{2}}\,\sqrt{||\mathfrak{s}||^2 + \widehat{\alpha}_\phi^2(\beta_p)} - \widehat{\beta}_\phi(p,\beta_p) \quad \text{with} \quad \boldsymbol{\sigma} = p\boldsymbol{1} + \mathfrak{s} \quad \text{and} \quad \beta_p = (M_{\phi\,\infty} - M_{\phi\,0})[1-\exp(-\alpha/\bar{\eta})] \tag{5}$$

governed by the logarithmic stress $\boldsymbol{\sigma}$ and the additional term $\widehat{\alpha}_\phi$ which provides a *smoothing-out of the peak* of the cone

$$\widehat{\alpha}_\phi(\beta_p) = \widehat{M}_\phi(\beta_p)\,\omega \quad \text{with} \quad \widehat{M}_\phi(\beta_p) = M_\phi + \beta_p \quad \text{and} \quad M_\phi = \frac{6\sin\Phi}{3 \pm \sin\Phi} \tag{6}$$

with the pressure-dependent material function in terms of the slope M_ϕ and the perturbation parameter ω defined as

$$\widehat{\beta}_\phi(p,\beta_p) = \widehat{M}_\phi(\beta_p)\,(p_{max} - p) \quad \text{with} \quad p_{max}^* := p_{max} - \sqrt{\tfrac{3}{2}}\,\omega \quad \text{and} \quad p_{max} = c\cot\Phi \tag{7}$$

where Φ is the friction angle and c is the cohesion of the Mohr–Coulomb criterion $|\tau| \leq c - p\tan\Phi$. In order to define the flow direction of the non–associated model, we introduce the plastic potential function

$$\widehat{\chi} = \sqrt{\tfrac{3}{2}}\,\sqrt{||\mathfrak{s}||^2 + \widehat{\alpha}_\chi^2} - \widehat{\beta}_\chi(p) \quad \text{with} \quad \widehat{\alpha}_\chi = M_\chi\,\omega \quad ; \quad \widehat{\beta}_\chi(p) = M_\chi\,(p_{max} - p) \quad \text{and} \quad M_\chi = \frac{6\sin\nu}{3 \pm \sin\nu} \tag{8}$$

in terms of the constant slope of the plastic potential hypersurface M_χ and the angle of dilatancy ν.

* Corresponding author: Email fadi.aldakheel@mechbau.uni-stuttgart.de, phone +49 711 685 66380, fax +49 711 685 66347

2 Balance equations of finite elasto-plasticity coupled with phase field fracture

The strong form of the balance and evolution equations describing the multi-field approach to phase-field-type crack propagation in inelastic soil mechanics are: Balance of linear momentum and evolution of the crack phase field corresponding to the *global fields* $\{\boldsymbol{\varphi}, d\}$, the evolution equation of α and evolution of the plastic strain $\boldsymbol{\varepsilon}^p$ corresponding to the *local fields*

$$\begin{aligned} &\text{Div}\,[\partial_{\nabla\boldsymbol{\varphi}}\widehat{\Psi}] = \boldsymbol{0} \quad , \quad \eta\dot{d} - (1-d)\mathcal{H} + [\,d - l^2\Delta d\,] = 0 \\ &\dot{\boldsymbol{\varepsilon}}^p - \lambda\,\partial_{\boldsymbol{\sigma}}\widehat{\chi}(\boldsymbol{\sigma}) = \boldsymbol{0} \quad , \quad \dot{\alpha} - \lambda\sqrt{\tfrac{2}{3}}\,||\partial_{\boldsymbol{\sigma}}\widehat{\chi}(\boldsymbol{\sigma})|| = 0\;, \end{aligned} \tag{9}$$

based on the *history field* $\mathcal{H}$ defined as the maximum of the *crack driving state function* D proposed in [1, 4]

$$\mathcal{H} = \max\, D(\boldsymbol{X}, s) \quad \text{and} \quad D = \zeta \left\langle \frac{\psi_e^+ + \psi_p}{\psi_c} - 1 \right\rangle \tag{10}$$

in terms of the *critical fracture energy per unit volume* ψ_c and the fracture length scale parameter l. The fracture parameter ζ controls the post-critical range after crack initialization.

3 Numerical examples

We point out the capabilities of the model by investigating the *pullout behavior of an anchor plate in soil* as shown in the experimental results [5]. The geometric setup and boundary conditions are illustrated in Figure 1 (a). Due to the symmetry of the BVP only half of the specimen is discretized using the modified enhanced assumed strain element CG4 in the simulation, which is proven to be a locking-free element and overcomes hourglass modes [6]. Figure 1 (b,c) demonstrate the distribution of the crack phase field d and the hydrostatic pressure p at the final deformation state. Tensile stresses are observed under the lower side of the anchor plate when the plate is pulled upwards. The crack starts to initiate in this tensile area when the elastic and plastic energies reach a critical value ψ_c and propagates from the anchor corners to the boundaries at about $60°$ from the loading direction. For visualization of the crack surface, deformed regions with $d \approx 1$ are not plotted in Figure 1 (c).

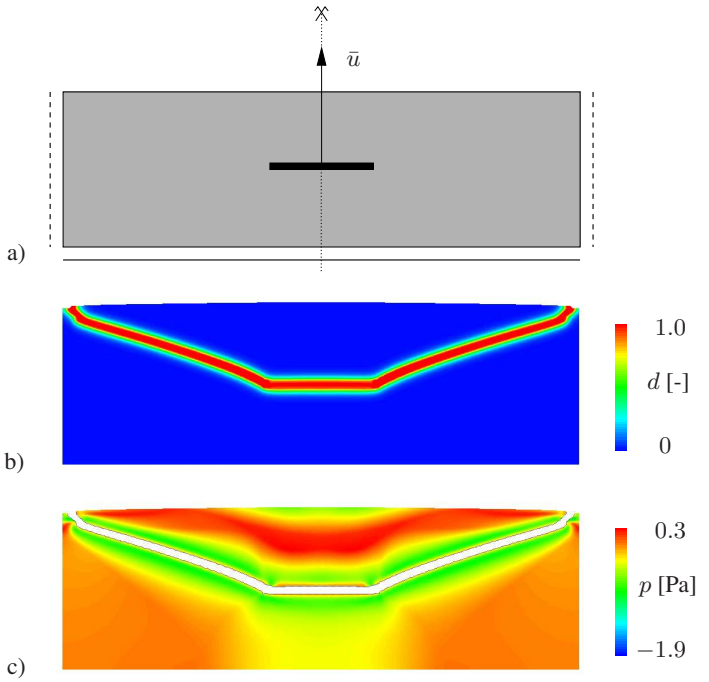

Fig. 1: Pullout behavior of anchor plate in soil. a) Geometry and boundary conditions, b) crack phase field d and c) hydrostatic pressure distribution p at the final stage of deformation.

References

[1] C. Miehe, D. Kienle, F. Aldakheel, S. Teichtmeister, Comput. Methods Appl. Mech. Engrg. **312**, 3–50 (2016).
[2] C. Miehe, M. Hofacker, L.-M. Schänzel, F. Aldakheel, Comput. Methods Appl. Mech. Engrg. **294**, 486–522 (2015).
[3] M. Lambrecht, C. Miehe, Acta Mech. **135**, 73–90 (1999).
[4] F. Aldakheel, Ph.D. thesis. http://dx.doi.org/10.18419/opus-8803 (2016).
[5] P. Bhattacharya, D. Bhowmik, S. Mukherjee, B. Chattopadhyay, 12th IACMAG, 3441–3447 (2008).
[6] J. Korelc, U. Solinc, P. Wriggers, Comput. Mech. **46**, 641–659 (2010).

